Optics Letters

Efficient four-wave mixing based on multiple plasmonic resonance

Junying Wang, Bokun Lv, Dahe Liu, Wenping Gong, and Jinwei Shi*

Department of Physics and Applied Optics Beijing Area Major Laboratory, Beijing Normal University, Beijing 100875, China
**Corresponding author: shijinwei@bnu.edu.cn*

Received 17 June 2021; revised 3 August 2021; accepted 14 August 2021; posted 18 August 2021 (Doc. ID 434231); published 7 September 2021

Plasmonic nanostructures provide a new way to improve nonlinear optical effects. As a mode of surface plasmons (SP), localized SPs can highly localize and enhance electromagnetic fields within a subwavelength volume. In this work, we developed a one-dimensional V-groove Ag nanograting. Through simulation, we realized triple-resonance enhanced four-wave mixing (FWM), in which both the excitation and signal waves are in resonance with LSPRs modified by propagating SPs, and can perfectly overlap with each other in each single nanogroove. Compared with that from a flat Ag plate, the FWM enhancement factor can be over six orders of magnitude. Next, we filled the Ag V-groove with nonlinear polymer 2-methoxy-5-(2-ethylhexyloxy)-1,4-phenylenevinylene and further improved the enhancement factor to eight orders of magnitude, together with a conversion efficiency of 1.02×10^{-2}. Finally, by changing the water filling ratio, the FWM signal is tuned over 180 nm, while keeping the enhancement factor over seven orders of magnitude.

https://doi.org/10.1364/OL.434231

As an important part of modern optics, nonlinear optics has special significance in optical frequency conversion. Since the invention of the laser, especially the discovery of second harmonic generation (SHG) [1], nonlinear optics has obtained great progress. As an important third-order nonlinear optical effect, optical four-wave mixing (FWM) has wide applications in wavelength conversion, signal regeneration, imaging, and so on [2–4]. However, due to limited interaction length, it is difficult to achieve highly efficient FWM in the micro- or nanometer scale.

The emergence of the metasurface has become a new platform for the study of nonlinear optics [5–9]. As one important type of metasurface, surface plasmons (SPs) can confine light to the surface of metal [10–13]. Therefore, the SP system is often used to study the interaction between light and matter. Localized SP resonance (LSPR) is a kind of non-propagating SP, which can generate a highly enhanced field compared with exciting far-field light. SPs, especially LSPR, have been widely used to enhance the conversion efficiency (CE), such as SHG, third harmonic generation (THG), and FWM [14–16]. Recently, many plasmonic structures have been proposed to enhance the CE of FWM, such as gap waveguide [17], nano cavity [18], metasurface [19], and double-resonance grating [20]. However, these structures suffer from a complex coupling structure, small radiation surface, or poor modal overlap, which greatly limits further enhancement and application of FWM.

In this work, in order to reduce the coupling complexity and keep the uniform surface-emitting property [20–23], we also adopted the simple grating structure to improve the CE of FWM. However, to increase the modal overlap, we adopted the nano V-groove structure and tuned the groove depth and pitch to achieve multiple resonances in one groove. Compared with that from a flat Ag plate, the FWM enhancement factor (EF) is over six orders of magnitude. Furthermore, by filling the Ag V-groove with nonlinear polymer 2-methoxy-5-(2-ethylhexyloxy)-1,4-phenylenevinylene (MEH-PPV), the EF is improved to eight orders of magnitude, together with a CE of 1.02×10^{-2}. Finally, by changing the water filling ratio, the FWM signal can be tuned over 180 nm.

In the following, as an example, we focus on the FWM process of $\omega_{\mathrm{FWM}} = 2\omega_a - \omega_b$. Figure 1(a) shows the energy level diagram of this FWM. The field distribution at the resonant wavelength is simulated by the finite-difference time-domain (FDTD) method. The electric field distribution within the structure is shown in Fig. 1(b). We can see that strong localized and enhanced electric field is formed in the grooves. Importantly, compared with the structure where different groove depth corresponds to different optical resonance [20], this structure can achieve better mode overlap of pump waves and FWM waves, which is the key factor to improve the nonlinear process [24,25]. To obtain the required LSPRs of the structure, we measured the reflectance spectra through FDTD simulation. The optimized groove depth is 560 nm, and the width on the surface is 50 nm. Experimentally, this structure can be fabricated by a focused ion beam. The optical parameters of Ag are taken from [26]. The polarization of the light source is perpendicular to the grooves. The dependence of the reflectance spectra to the pitch is shown in Fig. 1(c). Obviously, we can see two types of SP modes, one is the propagating SP polariton (SPP) in the lattice, and the other is LSPR. When these two kinds of modes come close to each other, strong coupling will take place, which can greatly alter the mode structure [27,28]. For nanophotonic application, the incident laser is usually tightly focused; therefore, a flat band in the momentum space

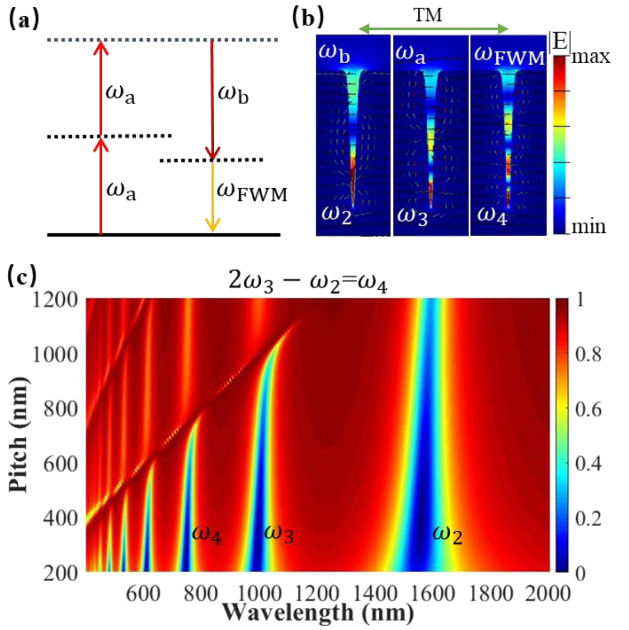

Fig. 1. Structure design principle. (a) Energy diagram of the specific FWM. (b) The electric field distribution within the grooves by simulation. $\lambda_2 = 1550$ nm, $\lambda_3 = 1010$ nm, $\lambda_4 = 748$ nm. The laser is TM polarized, as marked by the arrow. (c) The complete reflectance spectra with varying pitches. The 320 nm pitch corresponding to (b) is selected for further research.

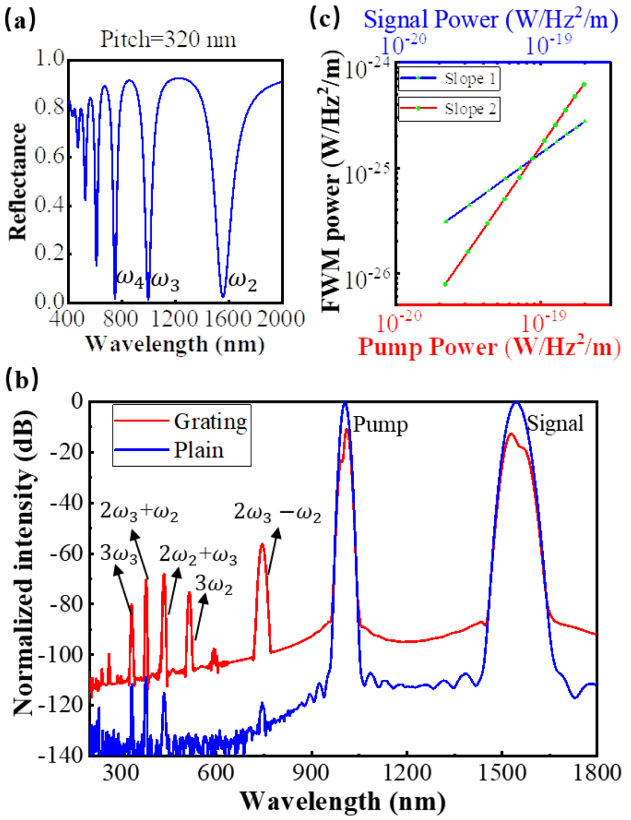

Fig. 2. Simulation results. (a) Reflectance spectra of the 320 nm pitch. (b) The extracted FWM power spectrum after normalization when the simulated light intensity is $I_2 = I_3 = 2.1 \times 10^{14}$ W/m^2. The red curve and the blue curve represent the power spectrum of the Ag nanometer grating and Ag plain, respectively. The y axis represents the logarithm of the ratio of the extracted FWM power to the pump power. (c) The generated FWM intensity with varying pump power and signal power.

is less sensitive to the incident angle. To realize such a flat band, the pitch is reduced so that basically only LSPR can exist in this structure. Notice that in nanogrooves the order of LSPR depends on the groove depth, but it is usually not equally spaced, because of the dispersion of SP. However, the detuned strong coupling can be used to modify the frequency spacing between the LSPR modes. By optimizing the grating parameters, one can always find a grating pitch where the 2nd, 3rd, and 4th LSPR modes are equally spaced, that is to say, $\omega_4 = 2\omega_3 - \omega_2$, which can be used to enhance the specific FWM in Fig. 1(a). Notice that the subscripts "2, 3, 4" represent the LSPR order. Changing the groove depth will change the order, but the relation in Fig. 1(a) is always correct.

By examining Fig. 1(c), we chose the pitch of the grating to be 320 nm. The reflectance spectrum is shown in Fig. 2(a), from which we can see that all three modes have a low reflectance, indicating strong near-field enhancement. Next, we introduced the third nonlinear into this structure. The third-order susceptibility of Ag is taken from [29]: $\chi^{(3)} = 2.8 \times 10^{-19}$ m^2/V^2. The nonlinear response is simulated by the FDTD method. The laser strikes the surface of the designed structure from the far field. Both the linear and nonlinear susceptibilities of the optical material are considered. After the light–matter interaction, the light carrying near-field information is radiated to the far field again. The far-field monitor records the outgoing time-dependent light field strength and obtains the signal power spectrum through time-domain Fourier transform. The normalized power spectrum is shown in Fig. 2(b), from which we can see all possible third-order processes on the high frequency side, including $2\omega_3 - \omega_2$, $2\omega_3 + \omega_2$, $2\omega_2 + \omega_3$, $3\omega_3$, $3\omega_2$. This is a typical property of nonlinear optics in the micro- and nanoscales, where phase matching is not important. Therefore, the competition of these processes only depends on modal resonances. In this structure, due to triple resonances, the process $\omega_4 = 2\omega_3 - \omega_2$ is dominant. The polarization of this special process is $P_{NL} = \varepsilon_0 \chi^{(3)}(\omega_4; \omega_3, \omega_3, -\omega_2) E_3 E_3 E_2^*$. The generated FWM intensity of ω_4 is plotted in Fig. 2(c) with varying pump power (ω_3) and signal power (ω_2). The slopes of these two lines are 1 and 2, consistent with the specific FWM process discussed here. From Fig. 2, the CE of this structure is $10^{-5.6}$, with an EF of $10^{6.26}$. The EF is obtained by comparing the signal from this structure with that from the Ag plate. The CE is defined as CE $= P_{FWM}/P_2$, where P_{FWM} is the FWM wave peak power, and P_2 is the signal power [17].

The obtained CE is still not satisfying, since only Ag contributes to the FWM. In order to achieve high CE, we filled the grooves with other nonlinear materials possessing high $\chi^{(3)}$. The nonlinear polymer has large third-order coefficient and small linear coefficient [30–33], which can be integrated to metallic nanostructures easily. In this work, a special polymer MEH-PPV is used as the filling material. One can fill the polymer into the nanogrooves by spin coating [17]. The optimal parameters are linear index of 1.65, depth of 480 nm, pitch of 500 nm, and groove width on the surface of 130 nm. The new reflectance spectrum is shown in Fig. 3(a). We can see that, under these parameters, the triple resonant condition is still fulfilled.

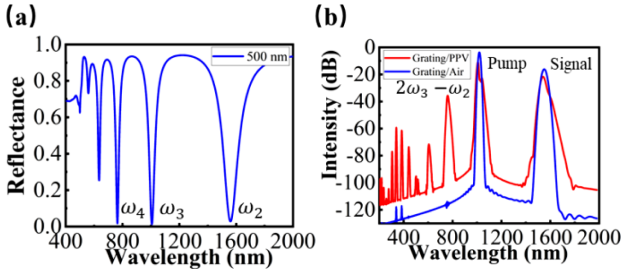

Fig. 3. Simulation results of highly efficient FWM. (a) Reflection spectrum of composite grating with a period of 500 nm. (b) The extracted FWM power spectrum. The red curve and the blue curve represent the power spectrum of the nonlinear polymer MEH-PPV grating and air-groove grating.

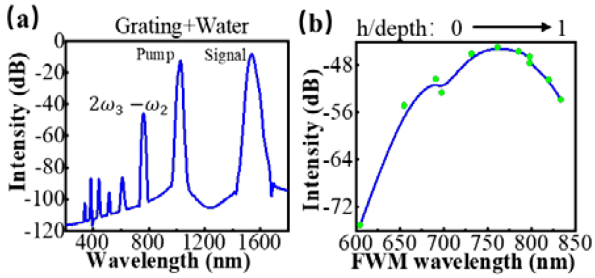

Fig. 4. (a) Power spectrum extracted from the composite structure of the grating filled with water. (b) The FWM wavelength and peak intensity change with the increase of water filling ratio. In (a) and (b), the simulated light intensity is $I_2 = I_3 = 2.1 \times 10^{14}$ W/m^2.

It is known that the polymer MEH-PPV could be damaged under a high power laser. Therefore, we set the peak intensities of the pump and signal laser to be $I_3 = 1.9 \times 10^{13}$ W/m^2 and $I_2 = 5.3 \times 10^{11}$ W/m^2. The nonlinear power spectrum is shown in Fig. 3(b), where the red curve denotes the structure with the polymer.

The FWM signal is enhanced by eight orders of magnitude, together with a CE of 1.02×10^{-2}. The values are greater than that in Fig. 2, close to real application. In literature, Michael *et al*. have done an excellent job and reported a higher CE of 4.67×10^{-2} using a slightly complicated plasmonic waveguide. However, in calculating the value, the coupling efficiency was not considered. Also, it was not a full surface-emitting device. The structure proposed here is easier to fabricate and to be applied, and this is a real surface-emitting device.

Finally, we study the tuning ability of this structure. To tune its optical response, we filled the grooves with water. We define the water height over the groove depth as the filling ratio. The filling ratio of water corresponds to the resonant wavelength of the LSPR. Experimentally, the filling ratio of water can be controlled by temperature, humidity, and laser intensity. One can also package the sample with polymer materials to prevent the loss of water. After optimization, the parameters are 460 nm depth, 260 nm pitch, 50 nm groove width on the surface, and, when the filling ratio is 0.5, the initial pump and signal laser are set at 1550 and 1024 nm, which generate the FWM at 763 nm. The third-order susceptibility of water is set as $\chi^{(3)}_{\text{Water}} = 2.5 \times 10^{-22}$ m^2/V^2 [34]. The nonlinear power spectrum is shown in Fig. 4(a). We can see that, using water as the filling nonlinear material, the CE can achieve $10^{-4.5}$.

If we fix the pump wave at 1550 nm, but vary the filling ratio from 0.1 to 1, the FWM can be tuned in a broad range by simultaneously changing the signal wavelength. The tuning result is shown in Fig. 4(b). In this case, most of the time this is a double resonant system, and the maximal CE is obtained at 763 nm, as shown in Fig. 4(a), which corresponds to the triple resonance. It can be seen that the CE of FWM is maintained above $10^{-5.6}$ from 650 to 830 nm (filling ratio 0.1–1), showing the wideband tunability of this structure.

On the other hand, if we fix both wavelengths of the pump laser and signal laser, due to the nonlinear response characteristics, the signal of FWM will be much more sensitive to the change of the filling ratio or, more generally, to the environmental parameters, than to the linear response of the plasmonic structure. This result indicates that the plasmon enhanced nonlinear FWM can be a great candidate for sensors with high sensitivity.

In summary, we realized enhanced FWM from the Ag grating with optimized parameters. The EF can be as large as $10^6 - 10^8$. This huge EF stems from LSPR-type multiple resonance and excellent spatial modal overlap. Furthermore, by filling the grooves with nonlinear polymer, the CE can be improved to 1.02×10^{-2}, which can be used for real application. Finally, by tuning the filling ratio of water in the groove, we are able to tune the FWM from 650 to 830 nm while maintaining a CE over $10^{-5.6}$. The method proposed here focuses on a specific FWM: $2\omega_3 - \omega_2 = \omega_4$. A similar idea can also be extended to other FWM or THG, as pointed out above. These finds may pave the wave to several applications, such as high-efficiency on-chip nonlinear frequency conversion, sensors with ultra-high sensitivity, etc.

Funding. National Natural Science Foundation of China (12174031, 91950108, 11774035, 11674032).

Disclosures. The authors declare no conflicts of interest.

Data Availability. Data underlying the results presented in this paper are not publicly available at this time but may be obtained from the authors upon reasonable request.

REFERENCES

1. P. A. Franken, A. E. Hill, C. Peters, and G. Weinreich, Phys. Rev. Lett. **7**, 118 (1961).
2. D. Klonidis, C. Politi, M. O'Mahony, and D. Simeonidou, IEEE Photon. Technol. Lett. **16**, 1412 (2004).
3. R. Salem, M. A. Foster, A. C. Turner, D. F. Geraghty, M. Lipson, and A. L. Gaeta, Nat. Photonics **2**, 35 (2007).
4. H. Kim, T. Sheps, P. G. Collins, and E. O. Potma, Nano Lett. **9**, 2991 (2009).
5. G. Li, S. Zhang, and T. Zentgraf, Nat. Rev. Mater. **2**, 17010 (2017).
6. J. Lee, M. Tymchenko, C. Argyropoulos, P. Y. Chen, F. Lu, F. Demmerle, G. Boehm, M. C. Amann, A. Alu, and M. A. Belkin, Nature **511**, 65 (2014).
7. L. Wang, S. Kruk, K. Koshelev, I. Kravchenko, B. Luther-Davies, and Y. Kivshar, Nano Lett. **18**, 3978 (2018).
8. Z. Liu, Y. Xu, Y. Lin, J. Xiang, T. Feng, Q. Cao, J. Li, S. Lan, and J. Liu, Phys. Rev. Lett. **123**, 253901 (2019).
9. Y. Dai, Y. Wang, S. Das, S. Li, H. Xue, A. Mohsen, and Z. Sun, Nano Lett. **21**, 6321 (2021).
10. M. A. Schmidt, D. Y. Lei, L. Wondraczek, V. Nazabal, and S. A. Maier, Nat. Commun. **3**, 1108 (2011).
11. M. E. Stewart, C. R. Anderton, L. B. Thompson, J. Maria, S. K. Gray, J. A. Rogers, and R. G. Nuzzo, Chem. Rev. **108**, 494 (2008).
12. W. L. Barnes, A. Dereux, and T. W. Ebbesen, Nature **424**, 824 (2003).
13. T. Liebermann and W. Knoll, Colloids Surf. A **171**, 115 (2000).

14. K. Thyagarajan, S. Rivier, A. Lovera, and O. J. F. Martin, Opt. Express **20**, 12860 (2012).
15. J. B. Lassiter, X. Chen, X. Liu, C. Ciracì, T. B. Hoang, S. Larouche, S. H. Oh, M. H. Mikkelsen, and D. R. Smith, ACS Photon. **1**, 1212 (2014).
16. P. Genevet, J. P. Tetienne, E. Gatzogiannis, R. Blanchard, M. A. Kats, M. O. Scully, and F. Capasso, Nano Lett. **10**, 4880 (2010).
17. M. P. Nielsen, X. Shi, P. Dichtl, S. A. Maier, and R. F. Oulton, Science **358**, 1179 (2017).
18. Q. Shen, W. Jin, G. Yang, A. W. Rodriguez, and M. H. Mikkelsen, ACS Photon. **7**, 901 (2020).
19. J. Boyuan and A. Christos, Sci. Rep. **6**, 28746 (2016).
20. M. L. Noordam, J. Hernandez-Rueda, L. Y. Talsma, and L. Kuipers, Appl. Phys. Lett. **116**, 101101 (2020).
21. C. Y. Wang, H. Y. Chen, L. Sun, W. L. Chen, Y. M. Chang, H. Ahn, X. Li, and S. Gwo, Nat. Commun. **6**, 7734 (2015).
22. J. Shi, W.-Y. Liang, S. S. Raja, Y. Sang, X.-Q. Zhang, C.-A. Chen, Y. Wang, X. Yang, Y.-H. Lee, H. Ahn, and S. Gwo, Laser Photon. Rev. **12**, 1800188 (2018).
23. Y. Ding, C. Wei, H. Su, S. Sun, Z. Tang, Z. Wang, G. Li, D. Liu, S. Gwo, J. Dai, and J. Shi, Adv. Opt. Mater. **9**, 2100625 (2021).
24. T.-Y. Chen, J. Obermeier, T. Schumacher, F.-C. Lin, J.-S. Huang, M. Lippitz, and C.-B. Huang, Nano Lett. **19**, 6424 (2019).
25. Y. Ogata, A. Vorobyev, and C. Guo, Materials **11**, 501 (2018).
26. E. D. Palik, *Handbook of Optical Constants of Solids* (Academic, 1998).
27. C.-Y. Wang, Y. Sang, X. Yang, S. S. Raja, C.-W. Cheng, H. Li, Y. Ding, S. Sun, H. Ahn, C.-K. Shih, S. Gwo, and J. Shi, Nano Lett. **21**, 605 (2021).
28. S. Sun, Y. Ding, H. Li, P. Hu, C.-W. Cheng, Y. Sang, F. Cao, Y. Hu, A. Alù, D. Liu, Z. Wang, S. Gwo, D. Han, and J. Shi, Phys. Rev. B **103**, 045416 (2021).
29. N. Bloembergen, W. K. Burns, and M. Matsuoka, Opt. Commun. **1**, 195 (1969).
30. T. J. Duffin, M. P. Nielsen, F. Diaz, S. Palomba, S. A. Maier, and R. F. Oulton, Opt. Lett. **41**, 155 (2016).
31. S. J. Martin, D. D. C. Bradley, P. A. Lane, H. Mellor, and P. L. Burn, Phys. Rev. B **59**, 15133 (1999).
32. J. M. Hales, J. Matichak, S. Barlow, S. Ohira, K. Yesudas, J.-L. Brédas, J. W. Perry, and S. R. Marder, Science **327**, 1485 (2010).
33. J. Semple, S. Rossbauer, C. H. Burgess, K. Zgao, L. K. Jagadamma, A. Amassian, M. A. Mclachlan, and T. D. Anthopoulos, Small **12**, 1993 (2016).
34. R. L. Sutherland, *Handbook of Nonlinear Optics* (Marcel Dekker, 1996), Chap. 8.